

Quantum Gravity Gradiometer Development for Space

James M. Kohel, Nan Yu, James R. Kellogg, Robert J. Thompson, David C. Aveline and Lute Maleki
 Jet Propulsion Laboratory, California Institute of Technology
 4800 Oak Grove Drive
 Pasadena, California 91109-8099

Abstract—Funded by the Advanced Technology Component Program, we have completed the development of a laboratory-based quantum gravity gradiometer based on atom interferometer technology. This is our first step towards a new space-borne gradiometer instrument, which can significantly contribute to global gravity mapping and monitoring important in the understanding of the solid earth, ice and oceans, and dynamic processes. In this paper, we will briefly review the principles and technical benefits of atom-wave interferometer-based inertial sensors in space. We will then describe the technical implementation of the laboratory setup and report its status. We will also discuss our implementation plan for the next generation instrument.

I. INTRODUCTION

GRAVITY field mapping is one of the key measurements required in order to understand the solid earth, ice and oceans, and dynamic processes in a comprehensive model of our planet. There have been a number of gravity measurement missions, such as CHAMP [1] and GRACE [2], which measure gravity through the precise monitoring of the relative motion of satellites or onboard drag-free test masses. Other gravity missions using mechanical gravity gradiometers have also been planned or are under development [3], [4].

We have proposed to develop an atom interferometer-based gravity for the measurement of the global gravity field from space [5]. Atom interferometry has proved a sensitive technique in laboratory-based measurements, and the operation of cold atom interferometers in space promises a significant enhancement of the inertial sensing performance due to the microgravity environment. As in gravity gradiometers based on mechanical accelerometers, the atom interferometer-based gravity gradiometer employs a differential acceleration measurement to allow cancellation as common-mode noise any vibrations of the reference platform. The application of atom interferometry to this differential measurement technique make possible the precise monitoring of absolute gravity fields from a moving platform such as a satellite.

As a first step in developing a gravity gradiometer for space, we have built a laboratory gradiometer system employing dual light-pulse atom interferometers. In this paper, we will first briefly review light-pulse atom interferometry and discuss briefly its application to gravity gradient measurements from space. We will then describe our laboratory system setup and implementation, and conclude with a summary of our current results and future plans.

II. QUANTUM GRAVITY GRADIOMETRY

The development of atom interferometers using laser light pulses [6], [7] has provided a sensitive new technique for inertial sensing. This technique employs laser-cooled atoms as identical drag-free test masses, unlike previous inertial sensors based on macroscopic test masses, and the de Broglie wave associated with each atom is then utilized to perform an interferometric measurement of the local acceleration. Light-pulse atom interferometers have already demonstrated impressive sensitivities in measurements of gravitational acceleration [8]–[10], rotations [10], [11] and gravity gradients [12] in the laboratory.

The quantum gravity gradiometer in our laboratory employs two cold atom interferometers using laser-induced stimulated Raman transitions [7] to measure differential accelerations along the vertical direction. The cesium atoms used in each atom interferometer are initially collected and cooled in two separate magneto-optic traps (MOTs). Each MOT, consisting of three pairs of counter-propagating laser beams along three orthogonal axes centered on a non-uniform magnetic field, collects up to 10^9 atoms. These atoms are then launched vertically as in an “atomic fountain” by switching off the magnetic field and introducing a slight frequency shift between pairs of lasers to create a moving rest frame for the trapped atoms. While still in this moving-frame molasses, the laser frequencies are further detuned from the atomic resonance (while maintaining this relative frequency shift) to bring the atom cloud’s temperature down to about $2 \mu\text{K}$, corresponding to an rms velocity less than 2 m/s.

After launch, the cold atoms undergo further state- and velocity-selection. The one-dimensional velocity selection is necessary to obtain good contrast by ensuring the Doppler broadening for the selected atoms is less than the transition linewidth for the Raman interferometer pulses. The $m_F = 0$ Zeeman sublevel is required to avoid the large linear magnetic field dependence. Both selections can be accomplished by employing a single narrow velocity-sensitive Raman π -pulse to drive the Cs $F = 4 \rightarrow 3, m_F = 0 \rightarrow 0$ transition [13]. The remaining atoms are pushed away using a short laser pulse resonant with atoms in the $F = 4$ level. Two additional microwave π -pulses and resonant laser clearing pulses are subsequently used to improve the Zeeman state selection and to return atoms to the $F = 3, m_F = 0$ state for interferometry.

The atom interferometers are realized by using a $\pi/2$ - π -

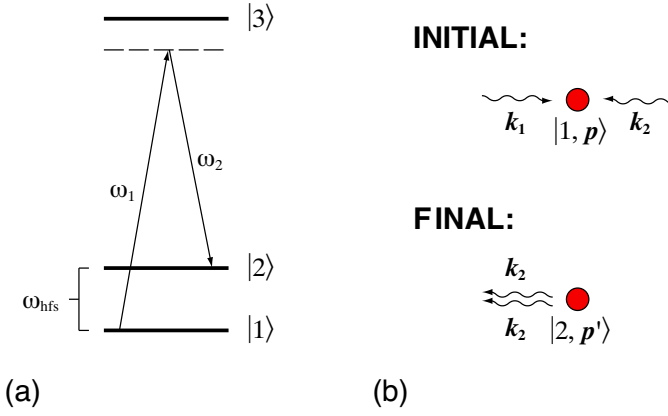


Fig. 1. Illustration of stimulated Raman transitions: (a) Energy level diagram for the atom, showing the Raman laser frequencies ω_1 and ω_2 . (b) Initial and final states for the atom coupled to the Raman lasers with wavenumbers \mathbf{k}_1 and \mathbf{k}_2 . The final momentum for the atom is $\mathbf{p}' = \mathbf{p} + \hbar(\mathbf{k}_1 - \mathbf{k}_2) \approx \mathbf{p} + 2\hbar\mathbf{k}_1$.

$\pi/2$ laser pulse sequence to drive velocity-sensitive stimulated Raman transitions between the two ground hyperfine states in cesium atoms in both interferometers (Fig. 1). The counter-propagating Raman laser beams are oriented along the vertical launch axis, parallel to the direction of gravitational acceleration to be measured. The first $\pi/2$ pulse at time t_1 creates an equal superposition of atoms in the two hyperfine ground states. Only the excited state receives a photon recoil kick and therefore travels at a slightly different velocity, realizing a beam splitting analogous to that in a traditional Mach-Zehnder interferometer. Subsequent π and $\pi/2$ pulses at times $t_2 = t_1 + T$ and $t_3 = t_1 + 2T$, respectively, similarly redirect and recombine the atom waves to complete an interferometer loop, as illustrated in Fig. 2. The transition probability resulting from this interferometer sequence is given by $P = \frac{1}{2} [1 - \cos(\Delta\phi)]$, where $\Delta\phi$ is the net phase difference between the two interferometer paths. This phase difference can be calculated from the Raman laser phases at the time and location of each interaction, i.e. $\Delta\phi = \phi(t_1, z_1) - 2\phi(t_2, z_2) + \phi(t_3, z_3)$. It can be further shown that the phase shift $\Delta\phi$ is related to the acceleration \mathbf{a} according to $\Delta\phi = \mathbf{k}_{\text{eff}} \cdot \mathbf{a}T^2$, where T is the time between pulses and $\mathbf{k}_{\text{eff}} \equiv \mathbf{k}_1 - \mathbf{k}_2 \approx 2\mathbf{k}_1$ is the effective Raman laser wave number. The acceleration \mathbf{a} is a vector sum of the gravitational acceleration \mathbf{g} and platform acceleration \mathbf{a}_p .

The atom interferometer phase shift can be measured by detecting the relative populations of the two hyperfine ground states via laser-induced fluorescence. The observed normalized signal takes the form of $P(\Delta\phi) = P_{\text{min}} + \frac{1}{2}A [1 - \cos(\phi_0 + \Delta\phi)]$, where A is the normalized fringe amplitude $P_{\text{max}} - P_{\text{min}}$. To illustrate the sensitivity of a single such interferometer, consider a measurement with interrogation time $2T = 1$ s. As little as $3 \times 10^{-8}g$ of acceleration will cause a fringe phase shift of one full radian, and the acceleration measurement sensitivity will be determined by the SNR in the fringe measurement. A recent laboratory measurement demonstrated a sensitivity of $2 \times 10^{-8}g \text{ Hz}^{-1/2}$ and $1 \times 10^{-10}g$ resolution after two days integration [9].

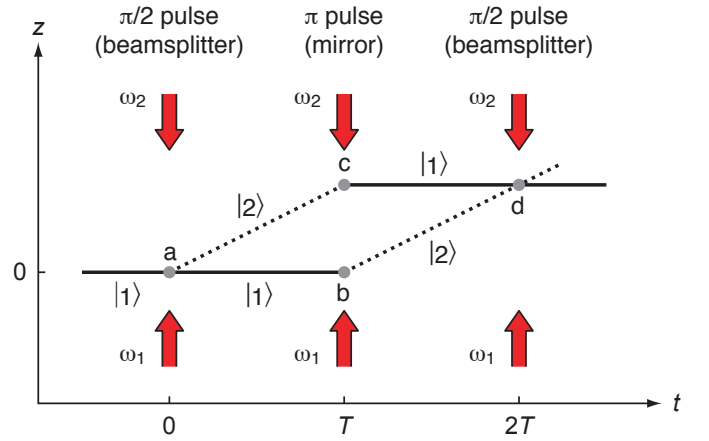


Fig. 2. Light-pulse atom interferometer diagram.

Although the gravitational acceleration can be measured directly as described above, this measurement requires an inertial frame of reference (i.e., $a_p = 0$) that is difficult to realize, even in a laboratory environment. This difficulty is a consequence of Einstein's Equivalence Principle: i.e. that an acceleration of the reference frame is indistinguishable from the gravitational acceleration in a local measurement. Gravity gradiometry provides a more fundamental measure of the gravitational fields by measuring the gravitational acceleration *difference* between two locations using a common reference frame so that other noninertial accelerations are rejected as common-mode noise. In the quantum gravity gradiometer, the two acceleration measurements are performed simultaneously in two atom interferometers separated by a distance d by using the same Raman laser beams (Fig. 3), so that platform vibrations and laser fluctuations are effectively cancelled. The differential phase shift in the two atom interferometers gives the gravitational acceleration difference in the two locations so that the linear gravity gradient can be derived from the baseline distance d . With this configuration in a laboratory setting, a differential acceleration sensitivity of $4 \times 10^{-9}g \text{ Hz}^{-1/2}$ has been demonstrated with an effective common-mode rejection of 140 dB [12]. Scaling to a 10 m separation baseline, this corresponds to a gravity gradient sensitivity of $4 \text{ E Hz}^{-1/2}$ ($1 \text{ E} \equiv 10^{-9} \text{ s}^{-2}$).

A. Microgravity operation

The gradiometer measurement sensitivity increases with the square of the interrogation time, in contrast to the linear dependence for Fourier-transform-limited measurements in atomic clocks. In a ground-based experiment in an atomic fountain, the interrogation time is limited to a fraction of a second due to practical limitations in the physical height of the apparatus. In a microgravity environment, interrogation times are limited only by the slow thermal expansion of the laser-cooled atoms. Such a benefit in microgravity environment has been recognized in other experiments with cold atom clocks [14], [15]. Experiments using cold atom interferometers in space have also been proposed to test Einstein's general relativity as well as the Equivalence Principle [16].

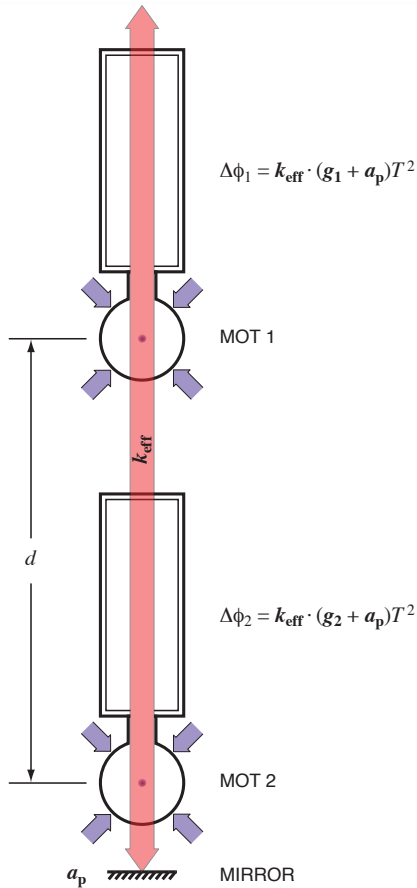


Fig. 3. Illustration of a gravity gradiometer based on dual atom interferometers. The Raman laser along the vertical axis measures the phase shift of atoms in each fountain, so that the gravity gradient along this axis is determined by $\Delta g/\Delta z = (\Delta\phi_1 - \Delta\phi_2)/(k_{\text{eff}}T^2d)$, and the platform vibrations a_p are effectively cancelled.

Due to the finite thermal velocity of atoms, the T^2 scaling is limited by the loss in the number of atoms when the interrogation time becomes long. The atom cloud volume expands as T^3 ; therefore, in the worse case of the atom loss limit, the SNR goes down as $T^{-3/2}$. As a result, the measurement sensitivity goes as $T^{1/2}$. An atom interferometer-based instrument, therefore, continues to gain in sensitivity at longer interrogation times despite the loss of atoms. This is in contrast with cold atom clocks where the sensitivity gain resulting from longer interrogation times is offset by the loss of atoms.

For gravity measurement in space, where 10 s interrogation times are conceivable, the measurement sensitivity can be enhanced by orders of magnitude over ground-based atomic fountains. As a result, a full radian phase shift corresponds to only a $7 \times 10^{-11}g$ of acceleration. Assuming a modest SNR of 100 with the currently achieved cooling temperature of $2 \mu\text{K}$, one achieves $1 \times 10^{-12}g$ of differential acceleration sensitivity in a single measurement sequence of about 20 s. A gradiometer with a baseline separation of 10 m would give a corresponding sensitivity about 1×10^{-3} E per single measurement, or roughly $0.004 \text{ E Hz}^{-1/2}$. Recently demonstrated techniques for improved laser cooling [17] and atom interferometry [18]

may be employed to further improve sensitivity with such long-baseline measurements.

We also note that the atom interferometer acceleration measurement can be treated as a more sophisticated spectroscopic measurement as in an atomic clock. The similarity and differences were clearly pointed out in the Ramsey-Borde interferometer scheme [6]. With longer than 20 s of total interrogation time, the Raman laser difference frequency stability has to be better than 1×10^{-12} at 10 s to achieve the above acceleration measurement sensitivity. The phase noise in the Raman lasers is common to both atom interferometers, however, and therefore is largely rejected as common-mode noise in the differential phase measurement.

III. LABORATORY INSTRUMENT DEVELOPMENT

A. Atomic physics package

The laboratory gradiometer consists of two atom-interferometer accelerometers separated by 1.4 m in the vertical direction. Each accelerometer operates in an atomic fountain configuration. The atomic fountains are housed in ultra-high vacuum (UHV) enclosures, which make the core part of the atomic physics packages (APPs). The first vacuum system, APP-1, was constructed from commercial off-the-shelf parts as a first testbed. It operates as a Cs vapor cell, and atoms are collected and trapped from the Cs background vapor. The second, APP-2, is an all-titanium (Ti) vacuum enclosure with welded optical windows (see Fig. 4). It has pairs of optical windows along the $[1,1,1]$ axes for the MOT beams. There are three additional windows and three vacuum pump ports inter-spaced between these six windows. Four more windows are located in the mid-plane 90 degrees apart. These additional windows are for diagnostic purposes; only eight of the thirteen windows are necessary for typical operation. Two separate large 75-mm diameter windows are located on the top and bottom for the Raman laser beams for interferometry. These are high-quality ($\lambda/20$ flatness) windows vacuum-sealed with copper knife-edge gaskets [19].

In the newer interferometer (APP-2), we collect cesium atoms from a background vapor in a separate higher-pressure source region and employ a series of 2D-MOTs as an “atom funnel” to load cold atoms into the UHV MOT. The compact 2D MOT source has been described in detail elsewhere [20], so we will describe it only in brief here. The source region consists of small ($12 \text{ mm} \times 12 \text{ mm} \times 45 \text{ mm}$) vapor cell that is attached to the UHV chamber through a glass-to-metal seal. A hairpin coil surrounding the cell generates a quadruple magnetic field, and a series of beam splitting cubes and retro-reflecting mirrors produce a contiguous series of two-dimensional traps. The cesium pressure in this source region was optimized at about 4×10^{-7} Torr, and a 4 mm diameter graphite-lined differential pumping tube (aligned along the axis of the 2D-MOTs) allows the cesium pressure in the adjacent UHV region to be maintained below 10^{-11} Torr. Using three short (12.7 mm) 2D-MOT stages and a total of 20 mW laser power for the source, we achieved a UHV MOT loading rate of 8×10^8 atom/s.

The simplified geometry of APP-2 allows the processes of state-preparation and detection to be performed in the UHV

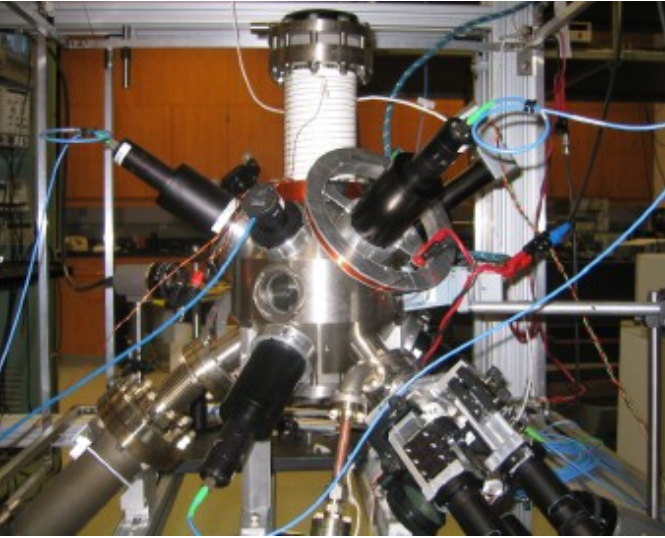


Fig. 4. Photograph of the atomic physics package APP-2. The 2D MOT cold atom beam source is also visible in the lower right quadrant.

MOT region using the same trap lasers. This compact design more closely corresponds to the the proposed microgravity instrument where long interrogation times can be obtained without operation as an atomic fountain. The UHV conditions afforded by loading this MOT from a cold atom beam (rather than a background vapor) also allow very low resonant background levels during detection.

B. Laser and optics subsystem

The laser and optical system (Fig. 5) for the quantum gravity gradiometer is designed to generate all the laser beams necessary for the simultaneous operation of the two atomic fountains and a 2D MOT source, as well as the beams for driving Raman transitions in the atom interferometers — a total of more than 20 laser beams with independent controls of frequency and intensity. All laser frequencies are referenced to a single master oscillator, consisting of a low power external cavity diode laser (ECDL), which is frequency-stabilized to the Cs $F = 4 \rightarrow 5'$ atomic transition using a saturation spectroscopy technique. The frequency lock has a loop bandwidth about 50 kHz, and is able to narrow the short-term linewidth to about 300 kHz ($\Delta f > 1$ MHz open loop). The phase noise spectrum of the locked laser indicates a sufficient laser frequency stability to achieve a SNR of 1000 with our detection scheme described below. The locked frequency stability goes down as $\tau^{-1/2}$ below 1 s, indicating white frequency noise. The stability reaches 6×10^{-13} at 1 s, and goes into the random walk regime at longer times. The long-term frequency stability is significant as it can induce additional noise in the differential atom interferometer phase measurement due to the Raman laser path length difference between the two interferometers [12].

The master laser power is preamplified by injection locking a higher power (50 mW) slave laser. From this preamplified laser beam, the required laser frequency shifts for the fountain operation and detection are made through use of doubled-

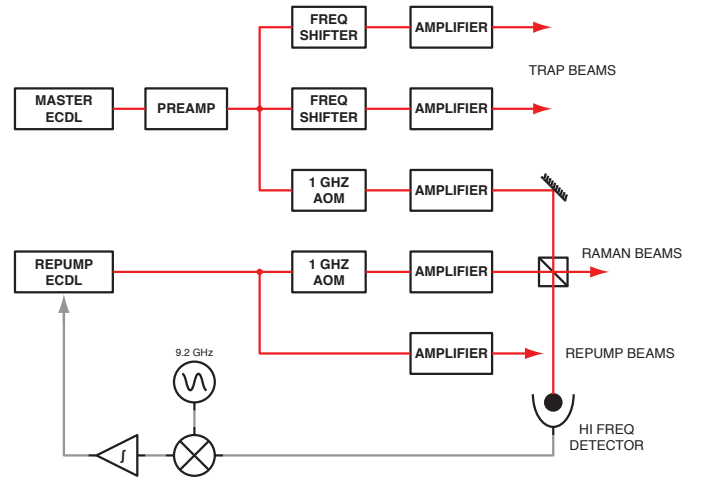


Fig. 5. Laser and optics system diagram.

passed acousto-optic modulators (AOMs). The frequency-shifted laser beams are subsequently power amplified by additional injection locked high power (150 mW) slave lasers. The $F = 3 \rightarrow 4'$ repump laser frequency is provided by a second ECDL phase-locked to the $4 \rightarrow 5'$ master laser with a frequency offset of 9.2 GHz (the spacing between the two Cs ground hyperfine states). This phase lock not only frequency-stabilizes the repump laser but, allows the generation of the phase-coherent laser beams to drive the Raman transitions. The repump laser is also further amplified by a slave laser. The Raman lasers are detuned from the resonance by 1.05 GHz using two high frequency AOMs, and amplified using two additional slave lasers.

We directly phase lock the output of the two Raman lasers using an electronic phase locked loop (PLL). The relative phase of the two lasers is detected by mixing the two laser fields in a fast photodetector. This beatnote is mixed down in two stages to the baseband, properly filtered, and fed back to one of the laser's frequency-control inputs. This first stage mixes down to an intermediate frequency around 100 MHz where all frequency and phase modulations are performed. In an atomic fountain, the freely falling atoms have a constant Doppler frequency chirp of $df/dt = -(k/2\pi)g \approx -23$ MHz/s. This Doppler shift is tracked by sweeping the frequency of the 100 MHz synthesizer in the phase locked loop. The phase locked loop has a frequency slow rate on the order of 1 GHz/s, more than sufficient for tracking the Doppler frequency chirp. When phase locked, the central peak contains 99% of the total RF power. From the beatnote spectrum measurement, we estimate the lock is tight within 1 mrad from 10 Hz to 100 kHz.

To implement a compact and robust laser system, we used functionally separate modules as building blocks [21]. The laser system consists of the following optical modules: master lasers, frequency lock modules, frequency shifters, slave lasers, and beam splitter/combiners. These modules are constructed using commercially available optical bench parts [22], and all modules are interconnected using polarization-maintaining optical fibers. Typical input-to-output

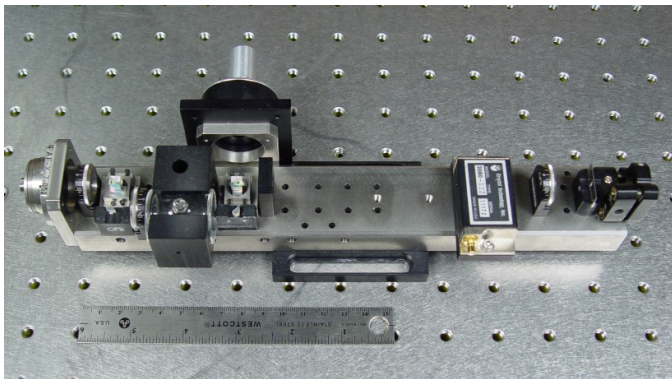


Fig. 6. Photograph of an optical module for laser frequency locking using FM saturation spectroscopy. Frequency modulation of the saturation beam is provided by the double-passed acousto-optic modulator. (FIP: fiber input port, HWP: half-wave plate, PBS: polarizing beam splitter, FL: focusing lens, AOM: acousto-optic modulator, QWP: quarter-wave plate, SL: slit aperture, M: mirror)

efficiencies within these modules are between 60% and 85%. According to the vendor, the output of optical benches made of these components is stable within 0.1 dB over changes in temperature from 20 °C to 70 °C, and the modules can survive 4g shock. The module shown in Fig. 6 is an example of a fiber-pigtailed laser frequency-locking module employing FM saturation spectroscopy in a Cs vapor cell. This module has a footprint of 5 cm \times 25 cm. The entire laser system sparsely occupies two 60 cm \times 90 cm breadboards.

IV. SYSTEM OPERATION AND RESULTS

The interferometer APP-2 employs a simplified design in which the state- and velocity-selection of atoms are performed in the trap region immediately after launch. In contrast, the original interferometer APP-1 is based on a vapor-cell MOT, and the state- and velocity-selection occurs after the atoms have left the trap region. In order to operate the interferometers simultaneously in the laboratory, we implemented an asynchronous launch sequence in which the second fountain (APP-2) launch is delayed until the launched atoms in the first fountain (APP-1) reach the state- and velocity-selection region. Atoms in the second fountain are then launched at a reduced velocity to match the mean velocity of the atoms in APP-1. Both atom interferometers operate synchronously from this point onward.

In both interferometers, up to 10^9 cold atoms are collected in the traps, and laser-cooled to about 2 μ K before launch. After state- and velocity-selection, we are typically left with less than 2% of the initial atom number for interferometry. This number is still sufficient to allow an atom number shot noise-limited SNR greater than 1000.

After undergoing the interferometer transition driven by the Raman laser pulses, the relative populations in the two hyperfine ground states are probed via laser-induced fluorescence. The measurement sequence consists of three detection laser pulses: (1) a 250 μ s $4 \rightarrow 5'$ standing-wave (SW) detection pulse to measure atoms in the $F = 4$ state, followed by a short $3 \rightarrow 4'$ repump pulse to transfer all atoms into the $F = 4$ state; (2) a second $4 \rightarrow 5'$ SW detection pulse to

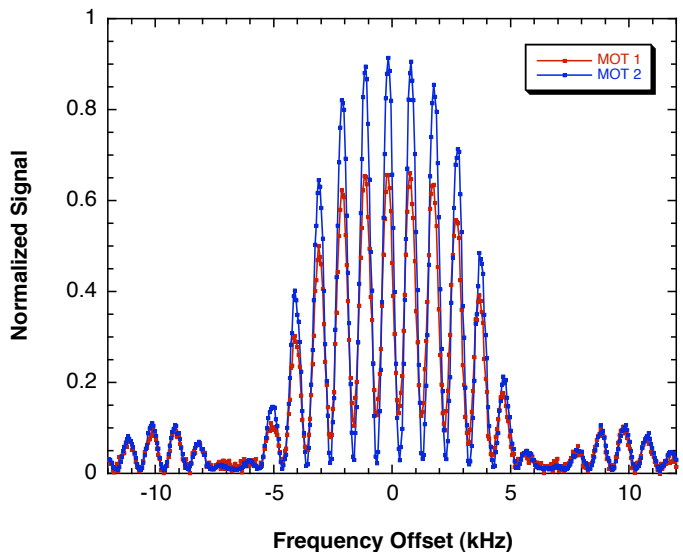


Fig. 7. Simultaneous measurement of Doppler-insensitive Ramsey spectra in the dual interferometers generated by using two Raman $\pi/2$ pulses separated by 1 ms. The data labelled MOT 2 is from the newer fountain APP-2.

measure the total atom signal, and finally (3) a third $4 \rightarrow 5'$ SW pulse following a long (20 ms) $4 \rightarrow 5'$ traveling-wave (TW) clearing pulse to measure the background signal due to non-resonant light scattering. The background signal measured by the third pulse is subtracted from first and second detection pulses to give the $F = 4$ populations and total atom numbers, respectively. To reduce the noise due to shot-to-shot variations in atom number, the $F = 4$ signal is normalized to the total atom number measured by the second pulse. In APP-2, the SW detection, repump, and TW clearing pulses are all generated from the MOT lasers.

The intrinsic SNR and systematics such as second-order Zeeman shifts and Stark shifts in the atom interferometers were characterized by configuring the Raman beams in a co-propagating geometry to drive velocity-insensitive Raman transitions. Fig. 7 shows a simultaneous measurement of the Ramsey fringes resulting from driving this Doppler-free clock transition in APP-1 and APP-2. We have achieved an initial SNR greater than 200 and Ramsey fringe contrast as high as 90% for short interrogation times.

Velocity-sensitive transitions in the atom interferometer are driven by Raman lasers in a counter-propagating Raman geometry. The phase of the interferometers, and therefore the final state populations, is dependent on atoms' acceleration relative to the retro-reflecting mirror along with any undesirable phase shifts in the Raman laser. To keep the Raman laser frequency in resonance with the falling atoms, a phase-continuous frequency chirp $\Delta\nu(t) = \gamma t$ is applied to the Raman laser frequency difference. The interferometer phase shift is then $\Delta\phi = k_{\text{eff}}(g + \gamma + a_p)T^2$. We use a commercially available passive vibration isolation platform to support the retro-optics. This platform has a low resonance frequency of about 1 Hz. With this passive isolation, we are able to observe atom interferometer fringes out to as long as 200 ms of total interaction time ($2T$). With no isolation the contrast is completely degraded within 2 ms

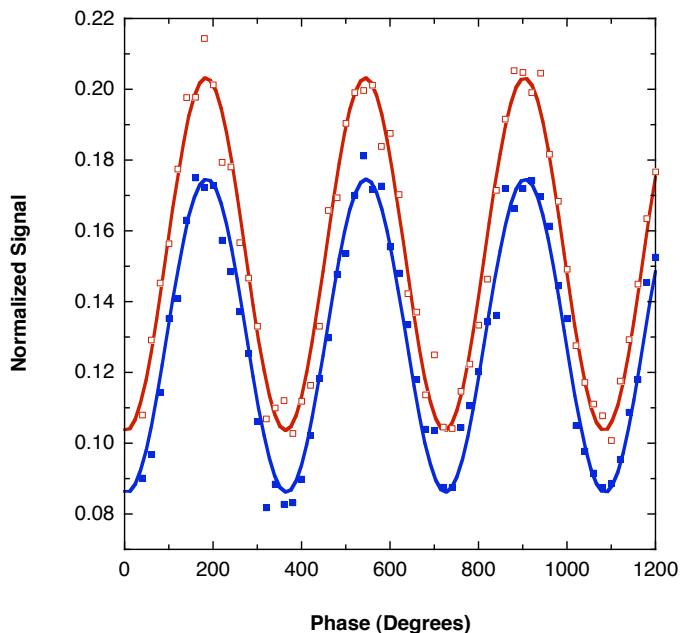


Fig. 8. Simultaneous measurements of atom interferometer fringes in two fountains. The Raman beam parameters were adjusted to compensate for the degraded window quality in APP-1 in order to make the two fringes equal in amplitude (see text).

of interaction time due to environmental noise. In fact, we are able to map out the residual vibration spectrum of the mirror on the isolation platform by measuring the fringe phase noise amplitudes at various interaction times. At 200 ms, we observe vibrations as little as 100 ng, corresponding to 1 nm of movement in the retro-optic platform during the interaction time. We are currently implementing an additional feed-forward compensation to the Raman laser phase for this environmental noise using an accelerometer on the vibration isolation platform [10]. This addition should greatly improve the individual interferometer fringe contrast and signal-to-noise ratios at very long interrogation times.

Fig. 8 shows the atom interferometer fringes recorded simultaneously in the two fountains. In principle, the phase difference in the fringe measurement yields the gravity gradient. Unfortunately, a degradation of the window coatings in APP-1 made it difficult to optimize signals and to characterize the other contributions to phase shift, such as the Stark effect, in the individual interferometers at the time of this measurement. Nevertheless, we can infer the system performance had we had two identical interferometers. With the demonstrated SNR of 200 and $T = 100$ ms, an acceleration measurement sensitivity of about $3 \times 10^{-9} g$ per measurement can be achieved. For our gradiometer separation of 1.4 m, we infer a gradiometer sensitivity of 34 E per measurement, or $34 \text{ E Hz}^{-1/2}$.

V. MOBILE INSTRUMENT DEVELOPMENT

We are also, as the next phase of this project, developing a compact mobile gravity gradiometer under NASA's Instrument Incubator Program. The mobile instrument is subject to additional design constraints in order to accommodate the requirements of size, weight, power consumption, robustness,

and cost; and here we only provide a partial summary of the ongoing effort satisfy these constraints in a high-sensitivity instrument.

The atomic physics package in the mobile instrument is being designed based on a [1,1,0] fountain geometry in a compact all-glass vacuum enclosure. The [1,1,0] geometry allows the horizontal MOT beams to be better optimized for detection, and also allows the anti-Helmholtz coils to be placed closer to the center of the trap to simplify the magnetic field requirements. A small ion pump in conjunction with a non-evaporable getter (NEG) will be sufficient to maintain the vacuum inside the UHV MOT region below the desired pressure of 10^{-9} Torr.

The next-generation laser system for this mobile instrument is based on the current modular design, but will employ a monolithic design for the individual modules to provide improved thermal and mechanical stability. We have also reduced the complexity of the optical system by implementing an offset frequency lock scheme. In this scheme, one reference laser is frequency locked to the Cs $F = 3 \rightarrow 4'$ transition while two additional master lasers are phase locked to the reference with a variable offset frequency. This offset frequency provides the frequency agility required by the lasers for atom collection, sub-Doppler cooling, interferometry, and detection, thus eliminating the frequency shift modules in the current laser system. The frequency synthesis chain, which is referenced to a Hydrogen maser in the laboratory instrument, will incorporate a dielectric resonator oscillator (DRO) steered by a precision crystal oscillator in the mobile instrument.

VI. CONCLUSION

We have constructed an atom interferometer-based gravity gradiometer employing component technologies suitable for a future flight instrument. We observed simultaneous high-contrast Ramsey fringes in the laboratory with this system as part of the characterization of the instrument performance, and we have also performed initial measurements of the differential phase in the two atom interferometers. Based on our characterization of the single atom interferometer performance, we can infer a gravity gradient measurement sensitivity of $34 \text{ E Hz}^{-1/2}$, corresponding to a sensitivity of $5 \text{ E Hz}^{-1/2}$ for a 10 m measurement baseline.

We are at the same time studying the unique challenges related to microgravity operation and long-baseline measurements. Further development is underway to produce a mobile instrument for gravity gradient measurements in the field, with the ultimate goal of developing a flight-qualified system suitable for global gravity field mapping from space.

ACKNOWLEDGMENT

This research was carried out at the Jet Propulsion Laboratory, California Institute of Technology, under a contract with the National Aeronautics and Space Administration. Reference herein to any specific commercial product, process, or service by trade name, trademark, manufacturer, or otherwise, does not constitute or imply its endorsement by the United States Government or the Jet Propulsion Laboratory, California Institute of Technology.

REFERENCES

- [1] Ch. Reigber, *et al.*, “A high quality global gravity field model from CHAMP GPS tracking data and Accelerometry (EIGEN-1S),” *Geophys. Res. Lett.* **29**, 10.1029/2002GL015064 (2002).
- [2] B. D. Tapley, S. Bettadpur, J. C. Ries, P. F. Thompson, and M. M. Watkins, “GRACE measurements of mass variability in the Earth system,” *Science* **305**, 503 (2004).
- [3] <http://www.esa.int/export/esaLP/goce.html>
- [4] <http://www.physics.umd.edu/GRE/SGGs.htm>
- [5] N. Yu, J. M. Kohel, L. Romans and L. Maleki, “Quantum gravity gradiometer sensor for earth science applications,” *Earth Science Technology Conference 2002*, Pasadena, CA, June 11–13, 2002.
- [6] Ch. J. Bordé, “Atomic interferometry with internal state labeling,” *Phys. Lett. A* **140**, 10 (1989).
- [7] M. Kasevich and S. Chu, “Atomic interferometry using stimulated Raman transitions,” *Phys. Rev. Lett.* **67**, 181 (1991).
- [8] M. Kasevich and S. Chu, “Measurement of the gravitational acceleration of an atom with a light-pulse atom interferometer,” *Appl. Phys. B* **54**, 321 (1992).
- [9] A. Peters, K. Y. Chung, and Steven Chu, “High-precision gravity measurements using atom interferometry,” *Metrologia* **38**, 25 (2001).
- [10] F. Yver-Leduc, *et al.*, “Reaching the quantum noise limit in a high-sensitivity cold-atom inertial sensor,” *J. Opt. B* **5**, S136 (2003).
- [11] T. L. Gustavson, A. Landragin, and M. A. Kasevich, “Rotation sensing with a dual atom-interferometer Sagnac gyroscope,” *Class. Quantum Grav.* **17**, 2385 (2000).
- [12] J. M. McGuirk, G. T. Foster, J. B. Fixler, M. J. Snadden, and M. A. Kasevich, “Sensitive absolute-gravity gradiometry using atom interferometry,” *Phys. Rev. A* **65**, 033608 (2002).
- [13] M. Kasevich and S. Chu, “Atomic velocity selection using stimulated Raman transitions,” *Phys. Rev. Lett.* **66**, 2297 (1991).
- [14] D. B. Sullivan, *et al.*, “PARCS: NASA’s laser-cooled atomic clock in space,” *Adv. Space Res.* **36**, 107 (2005).
- [15] P. Lemonde, *et al.*, “Test of a space cold atom clock prototype in the absence of gravity,” *IEEE Trans. Instrum. Meas.* **48**, 512 (1999).
- [16] <http://sci.esa.int/hyper/>; Quantum Interferometer Einstein’s Equivalence Principle Test (QuITE), a study funded by NASA’s Fundamental Physics Program (2003).
- [17] A. J. Kerman, V. Vuletić, C. Chin, and S. Chu, “Beyond optical molasses: 3D Raman sideband cooling of atomic cesium to high phase-space density,” *Phys. Rev. Lett.* **84**, 439 (2000).
- [18] J. M. McGuirk, M. J. Snadden, and M. A. Kasevich, “Large area light-pulse atom interferometry,” *Phys. Rev. A* **85**, 4498 (2000).
- [19] A. Noble and M. Kasevich, “UHV optical window seal to conflat knife edge,” *Rev. Sci. Instrum.* **65**, 3042 (1994).
- [20] J. Ramirez-Serrano, N. Yu, J. M. Kohel, J. R. Kellogg, and L. Maleki, “Multistage two-dimensional magneto-optical trap as a compact cold atom beam source,” *Opt. Lett.* **31**, 682 (2006).
- [21] N. Yu, J. M. Kohel, J. Ramirez-Serrano, J. R. Kellogg and L. Maleki, “Progress towards a space-borne quantum gravity gradiometer,” *Earth Science Technology Conference 2004*, Palo Alto, CA, June 22–24, 2004.
- [22] Optics For Research, Inc., Caldwell, New Jersey 07006.